# Spin-label EPR on Disordered and Amyloid Proteins

Hashemi Shabestari, M.

# *CHAPTER 1*

# INTRODUCTION

This chapter is a general introduction to the work presented in this thesis. A brief overview of the techniques used and the proteins investigated is provided. At the end, the outline of the chapters of the thesis is given.

# 1 Introduction

Proteins are essential for organisms and participate in virtually every process within cells [1]. Knowledge about the structure of proteins provides crucial information about their function in biological mechanisms. In determining the structure of proteins with biophysical approaches, electron paramagnetic resonance (EPR) is rapidly gaining ground [2-13]. The aim of this thesis is to provide insight in how broad the application of EPR can be to study proteins, in particular those which are difficult if not impossible to study with other approaches. The focus of this thesis is to investigate the aggregation and misfolding of intrinsically disordered proteins and to determine the structure of disordered parts of proteins with EPR. Specifically, the amyloid β (Aβ) peptide, the α-synuclein (αS) protein, and the light-harvesting protein CP29 are studied. In the present chapter, the basic theory of EPR spectroscopy is described and an overview of the proteins studied is provided.

## 1.1 Introduction to EPR spectroscopy

### 1.1.1 Zeeman interaction and hyperfine interaction

In EPR spectroscopy, transitions between the spin levels of a paramagnetic system are induced by electromagnetic radiation in a static magnetic field [14,15]. The interaction between the electron spin, $\vec{S}$, and the external magnetic field is called the electron Zeeman interaction ($H_{EZ}$). In the presence of the external magnetic field, the electron spin occupies one of two states, which can be thought of as the electron spin aligned with or against the magnetic field.
In addition to the Zeeman interaction, the electron spin experiences a small local magnetic field produced by nearby nuclei. This interaction is known as the hyperfine interaction ($H_{HF}$), and may counter or enhance the externally applied field. Taking into account the Zeeman interaction and the hyperfine interaction with one nuclear spin, $\vec{I}$, the spin Hamiltonian can be written as:

$$H = H_{EZ} + H_{HF} = \beta_e \vec{B}_0 \overleftrightarrow{g}_e \vec{S} + \vec{S} \overleftrightarrow{A} \vec{I} \qquad (1.1)$$

Here $\beta_e$ is the Bohr magneton, $\vec{B}_0$ is the external magnetic field, $\overleftrightarrow{g}_e$ is the g-tensor, and $\overleftrightarrow{A}$ the hyperfine tensor. Figure 1.1 shows the corresponding energy level scheme for a nitroxide spin label, which contains an electron spin (S = 1/2) and a nitrogen ($^{14}$N, I = 1) nuclear spin. In the magnetic field the degenerate $M_s$ = 1/2, -1/2 magnetic sublevels of the electron spin split up by the Zeeman interaction and a further splitting into three $M_I$ = 1, 0, -1 nuclear spin magnetic sublevels results from the hyperfine interaction. The EPR transitions correspond to transitions between

levels for which $|\Delta M_s| = 1$ and $\Delta M_I = 0$. For an isotropic g-tensor and an isotropic hyperfine tensor, the energy difference between the levels involved in the three transitions can be written as: $\Delta E = g_e \beta_e B_0 + A_{iso} M_I$ with $M_I$ = 1, 0, -1. The isotropic $g_e$ has the value of 2.00551 [16] and $A_{iso}$ of a nitrogen ($^{14}$N, I = 1) nuclear spin of a nitroxide spin label has the typical value of about 1.63 mT [16]. The transitions show up in the EPR spectrum at magnetic fields such that the resonance condition $\Delta E = h\nu$ is fulfilled, where h is Planck's constant (h = 6.626 × $10^{-34}$ Js) and ν the frequency of the electromagnetic radiation.

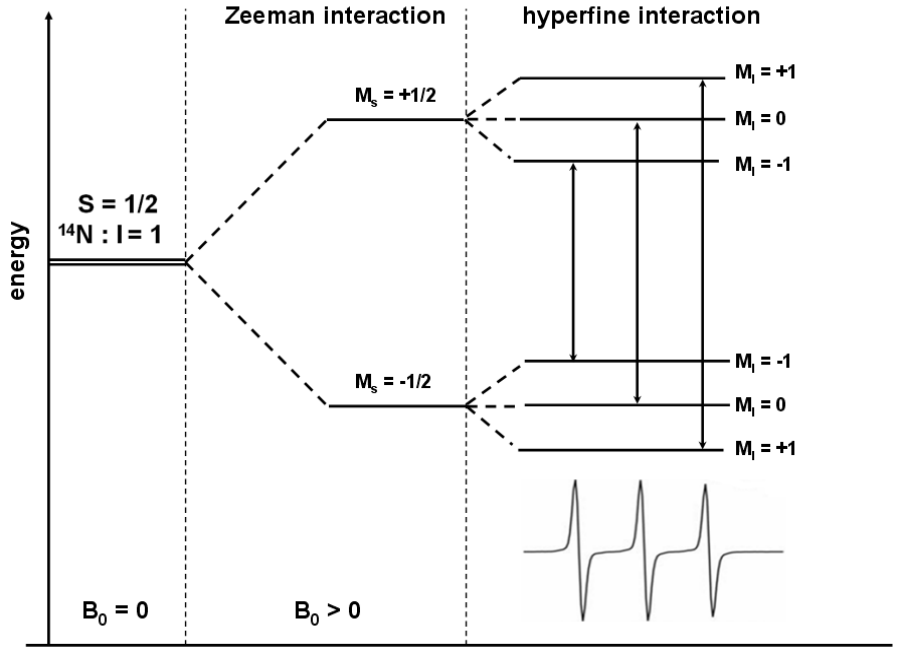


**Figure 1.1** Energy level scheme and allowed EPR transitions for an electron spin (S = ½) in interaction with a $^{14}$N nitrogen nuclear spin (I = 1). The hyperfine interaction leads to a splitting into 2I + 1 = 3 transitions, each corresponding to a $^{14}$N nuclear spin state ($M_I$ = −1, 0, +1).

For anisotropic g and hyperfine tensors, the orientation of the magnetic field with respect to the molecular system has to be taken into account [11]. The principal components of the hyperfine interaction tensor ($\vec{\vec{A}}$) are defined as $A_{xx}$, $A_{yy}$, and $A_{zz}$, those of the g-tensor as $g_{xx}$, $g_{yy}$, and $g_{zz}$. For nitroxide spin labels typical values of the hyperfine interaction of the nitrogen ($^{14}$N, I = 1) nuclear spin are $A_{xx} \approx A_{yy} \approx 0.7$ mT and $A_{zz} \approx 3.5$ mT. The isotropic hyperfine-coupling $A_{iso} = (A_{xx} + A_{yy} + A_{zz})/3$. The difference between $A_{xx}$ and $A_{yy}$ is small and often the hyperfine tensor is

assumed to be axially symmetric. The magnitude of $A_{zz}$ gives an indication of the polarity of the environment. In contrast to the hyperfine tensor, the g-tensor is rhombic with typical values of $g_{xx} \approx 2.00800$, $g_{yy} \approx 2.00586$, and $g_{zz} \approx 2.00199$ [11]. The anisotropy of the Zeeman and the hyperfine interactions determines the sensitivity of the EPR spectrum to the orientation and rotational motion of the spin label.

### 1.1.2 Spin labels for protein EPR

Spin labels are extrinsic paramagnetic probes, which are commonly nitroxide derivatives with a stable unpaired electron and a functional group that allows its site-specific attachment to a protein, site-directed spin labeling [11,17]. The nitroxide radicals are stable due to the presence of methyl groups adjacent to the nitroxide. Figure 1.2 shows the structure of the two nitroxide spin labels, which are used in this thesis: the MTS spin label ((1-oxyl-2,2,5,5-tetramethylpyrroline-3-methyl) methanethiosulfonate), and the non-coded nitroxyl-containing α-amino acid, TOAC (2,2,6,6-tetramethylpipe-ridine-1-oxyl-4-amino-4-carboxylic acid). The TOAC spin label serves as a rigidly attached spin label [18,19] compared to the rotationally flexible MTS spin label.

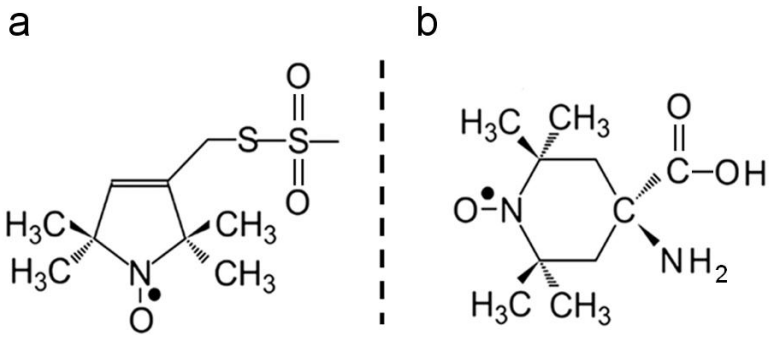


**Figure 1.2** The chemical structure of two nitroxide radicals. a: The MTS spin label. The NO group of the MTS spin label is part of a five-membered pyrrole ring. b: The TOAC spin label. The NO group of the TOAC spin label is part of a six-membered piperidine ring. The black dot represents the unpaired electron.

Rotational motions of the nitroxide lead to partial averaging of the anisotropy between the elements of the *g*-tensor and the hyperfine tensor, and give rise to variations in the observed cw-EPR spectrum. The cw-EPR spectrum of a nitroxide spin label can be used to infer information about the local environment of the labeling site. Through EPR analysis, it is possible to determine the local structure and dynamics, to map inter-residue distances, and to reconstruct the three-dimensional structure of proteins.

### 1.1.3 Dynamics by EPR: the rotation-correlation time

The shape of the EPR spectrum depends not only on the static interactions in the paramagnetic molecule, but also on the dynamic processes on the timescale of the EPR experiment. The EPR timescale is determined by the anisotropy of the g and A tensors of the molecule. These cause the spectral anisotropy, i.e., the maximum difference between resonance line positions when the orientation of the molecule is varied [17]. Any dynamic process on the timescale determined by the g and A tensor anisotropy will affect the shape of the EPR spectrum. The most important dynamic process in solution is the tumbling of the molecules, which is characterized by the rotation-correlation time $\tau_r$. Figure 1.3 shows the four dynamic regimes that are distinguishable [17,20].

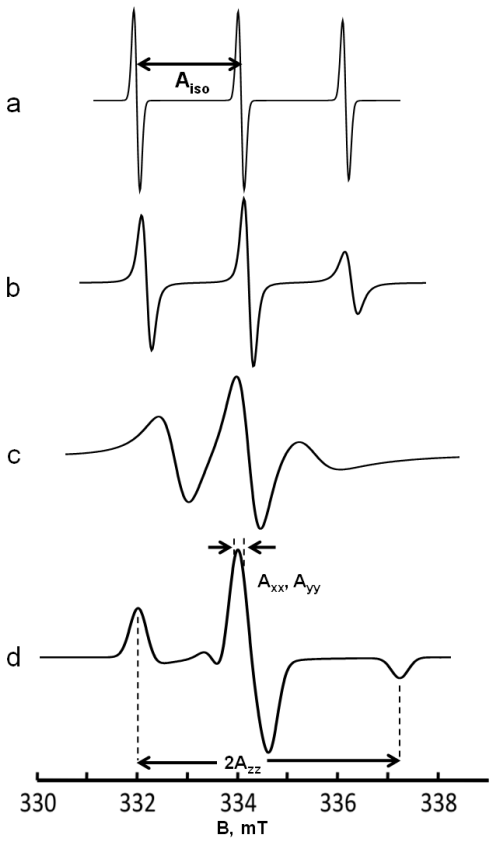


**Figure 1.3** Simulation of the effect of the rotation-correlation time on the line-shape of the EPR spectrum of a nitroxide spin label. In the isotropic limit the three lines have equal intensities. a: liquid solution EPR spectrum of the nitroxide spin label with $\tau_r$ = 0.1 ns. b: liquid solution EPR spectrum of the nitroxide spin label with $\tau_r$ = 0.4 ns. c: liquid solution EPR spectrum of the nitroxide spin label with $\tau_r$ = 2.2 ns. d: frozen solution EPR spectrum of the nitroxide spin label.

In the isotropic limit, the anisotropy is completely averaged due to the extremely fast tumbling of the molecules. The lines are symmetric and have an equal width and heights. In the fast-motion regime the rotation is fast enough to average the anisotropy, but the lines have different widths and heights. In the slow-motion regime, the rotation of the molecules is not fast enough to fully average the anisotropy. Therefore, the lines broaden and shift with respect to the isotropic limit. From the amount of spectral change, the rotation-correlation time can be obtained by simulation [20]. In the rigid limit, the molecules are randomly oriented with respect to the magnetic field and immobilized, and the EPR spectrum shows the full anisotropy. Line-shape analysis of EPR spectra reveals information about the local dynamics and possibly about the local structure elements of proteins [3,4,6].

### 1.1.4 Spin-spin interaction

Distance determination in biological molecules can be done by introducing spin labels at two positions and measuring the distance between the labels by EPR. The two labels can interact via two mechanisms: the exchange interaction, the magnitude of which is J, and the dipole-dipole interaction. The exchange interaction is related to the overlap of the orbitals that contain the two unpaired electrons. Depending on the magnitude of this orbital overlap, which is determined by the separation between the orbitals, the exchange interaction can cause multiplet spectra or line broadening. When the overlap is large, the two electron spins can be in two states: a singlet and a triplet state (S = 0, 1). The triplet state is lower in energy, thus we consider the two electron spins to be in the triplet state. In the presence of an external magnetic field the three $M_s$ = 1, 0, -1 magnetic sublevels of the triplet state split up by the Zeeman interaction. In the case of two nitroxides, owing to the presence of two nuclear spins: $M_I^1$ = 1, 0, -1, and $M_I^2$ = 1, 0, -1, a further splitting results from the hyperfine interaction (figure 1.4). Considering the allowed transitions ($|\Delta M_s| = 1$ and $\Delta M_I = 0$), in the strong exchange limit, where the ratio of $A_N/J$ is small, the spectrum contains five lines with intensities 1:2:3:2:1 with a spacing of one-half of the hyperfine coupling constant for the nitroxide spin label (figure 1.4). When the ratio of $A_N/J$ is one-half, the transitions between the singlet and the triplet state can be observed as satellite lines. When the ratio of $A_N/J$ increases, the transitions arrange into three groups of lines, and finally when the exchange interaction is weak, the three-line spectrum results, which is characteristic of a nitroxide spin label. Exchange interactions are usually negligible at distances beyond 1.5 nm.

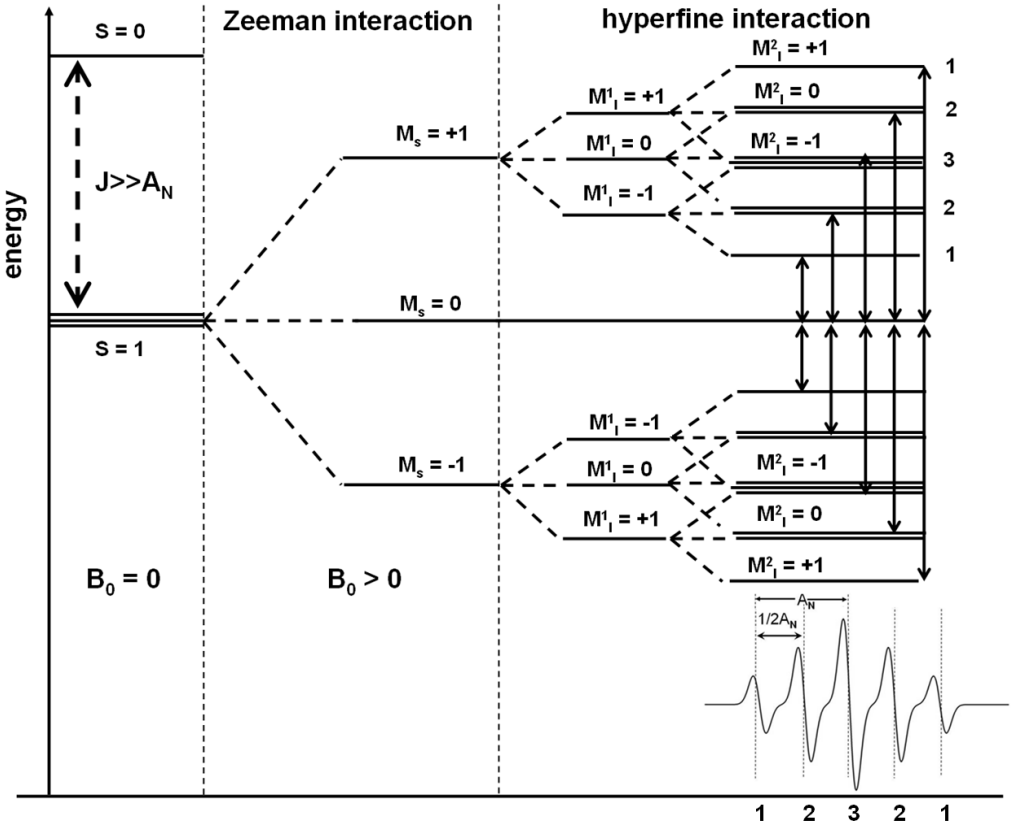


**Figure 1.4** Energy level scheme for the two electron spins (S = ½) and two nitrogen ($^{14}$N, I = 1) nuclear spins for J >> $A_N$. The spectrum contains five lines with intensities 1:2:3:2:1 with a spacing of one-half of the hyperfine coupling constant for the nitroxide spin label.

The dipole-dipole interaction is inversely proportional to the cube of the distance. The dipole-dipole interaction in frequency units, $\nu_{dd}$, between two spins A and B is given by:

$$\nu_{dd} = -\frac{\mu_0 \beta_e^2}{8\hbar\pi^2}\frac{g_A g_B}{r_{AB}^3}\left(3\cos^2\theta - 1\right) \qquad (1.2)$$

Here $g_A$ and $g_B$ are the isotropic g factors of the two electron spins, $r_{AB}$ is the magnitude of the vector that joins the two electrons, and θ is the angle between the magnetic field and the vector that joins the two electrons (figure 1.5). The dipole-dipole interaction causes line splitting or line broadening in cw EPR, which are resolved in nitroxides at spin-spin distances shorter than 1.5 nm [13,21].

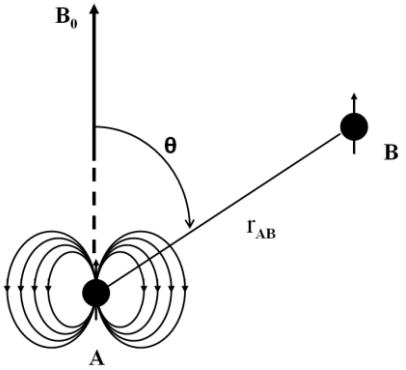


**Figure 1.5** Schematic representation of the dipole-dipole interaction in a magnetic field between two electrons A and B represented as black circles.

For nitroxide spin labels at distances larger than 2 nm the dipole-dipole interaction is not resolved in the cw EPR spectra. Long-range distances (2 to 8 nm) can be measured with pulsed double electron-electron resonance spectroscopy (DEER), also called PELDOR [22]. This technique is based on the detection of the modulation of the echo amplitude, caused by the dipolar interaction of two spins. Microwave pulses of two different microwave frequencies are used, where the two frequencies select different orientations or different spin states of the $^{14}N$ nucleus in the two radicals. The pulse sequence of the four-pulse DEER is shown in figure 1.6. At the observer frequency ($mw_1$), a refocused echo with a fixed position in time is detected for spins in resonance (spins A). Between the second and third pulse, an inversion pulse is applied at the pump frequency ($mw_2$), which flips the spins that are in resonance with the second frequency (spins B). Dipolar interaction between spins A and spins B results in the modulation of the amplitude of the refocused echo as a function of time, t (figure 1.7). The modulation frequency is given by equation 1.2. To determine the distance distribution for two sites within the same macromolecule, the contribution of the interactions of spins within the same molecule should be separated from the background contribution due to the interactions with spins in neighboring macromolecules. The echo signal is a multiplication of these two contributions.

Due to the flexibility of the macromolecules and conformational freedom of the spin label, the spin-spin distance is not always as sharply defined as in the rigid biradical shown in figure 1.7. In the case of proteins often broad distance distributions result, which will be addressed in chapters 5 and 6 of this thesis. The overall signal shows the superposition of modulations at different frequencies, rather than a single frequency. In that case separation of the background contribution from the modulation is improved by using an experimental background

function from the corresponding singly labeled protein (chapter 5). By means of regularization methods or model-based approaches, it is then possible to extract the distance distributions from the DEER time traces [23,24].

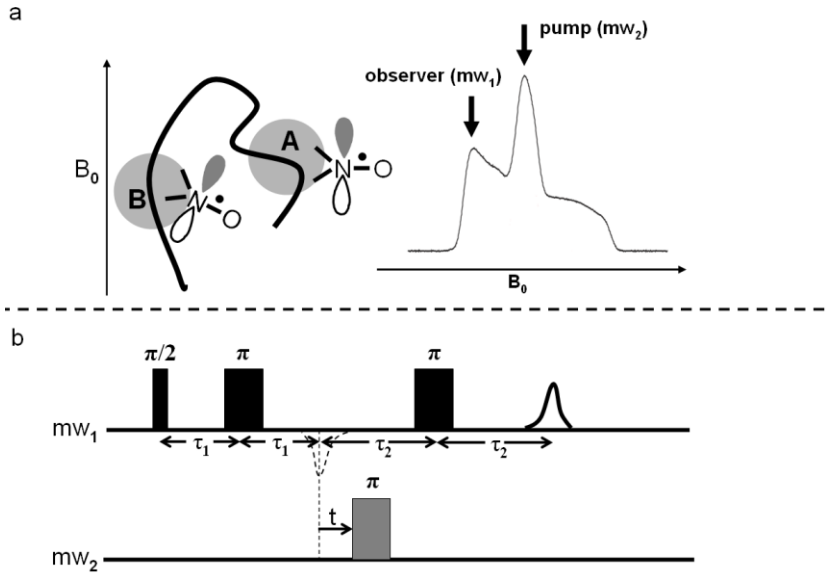


**Figure 1.6** The principle of double electron-electron resonance (DEER) spectroscopy. a: Right: absorption type EPR spectrum showing resonances of observed and pumped spins. Left: a macromolecule with two nitroxide spin labels, A and B. The two spin label N-O groups have different orientations with respect to the magnetic field, $B_0$. b: Pulse sequence of the DEER experiment consisting of the refocused echo sequence at frequency $mw_1$ that excites exclusively spins A and a pump pulse at frequency $mw_2$ that excites exclusively spins B. Delays $\tau_1$ and $\tau_2$ are fixed, and the amplitude of the echo is monitored while the time delay t is varied.

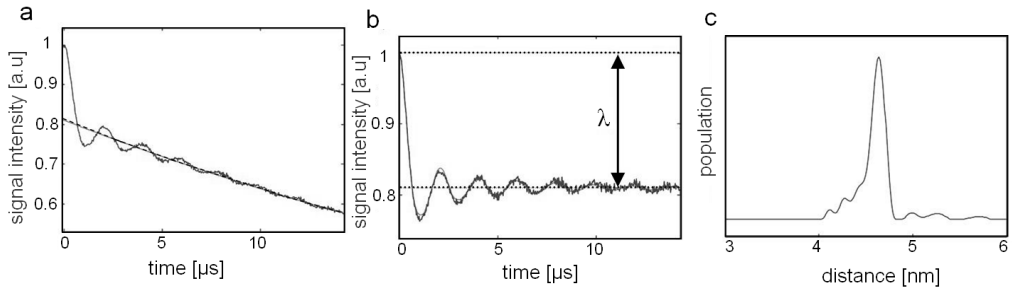


**Figure 1.7** Analysis steps of DEER distance measurement on a rigid biradical. a: Raw DEER time trace. The dashed line is the background fit. b: The background corrected DEER time trace. The modulation depth, λ is related to the fraction of coupled spins. c: Distance distribution obtained by the Tikhonov regularization method [25]. Small features are probably artifacts of the regularization at distances longer than 5 nm.

## 1.2 The proteins and their properties

### 1.2.1 Structure of proteins

Proteins are composed of amino-acid residues. Each amino-acid residue is connected to the next one by a peptide bond and forms the polypeptide chain. The order of the amino-acid residues in the polypeptide chain determines the primary structure of the protein. The secondary structure of the protein refers to the polypeptide folding patterns, which are classified as α-helices, β-sheets, turns and random coils (figure 1.7).

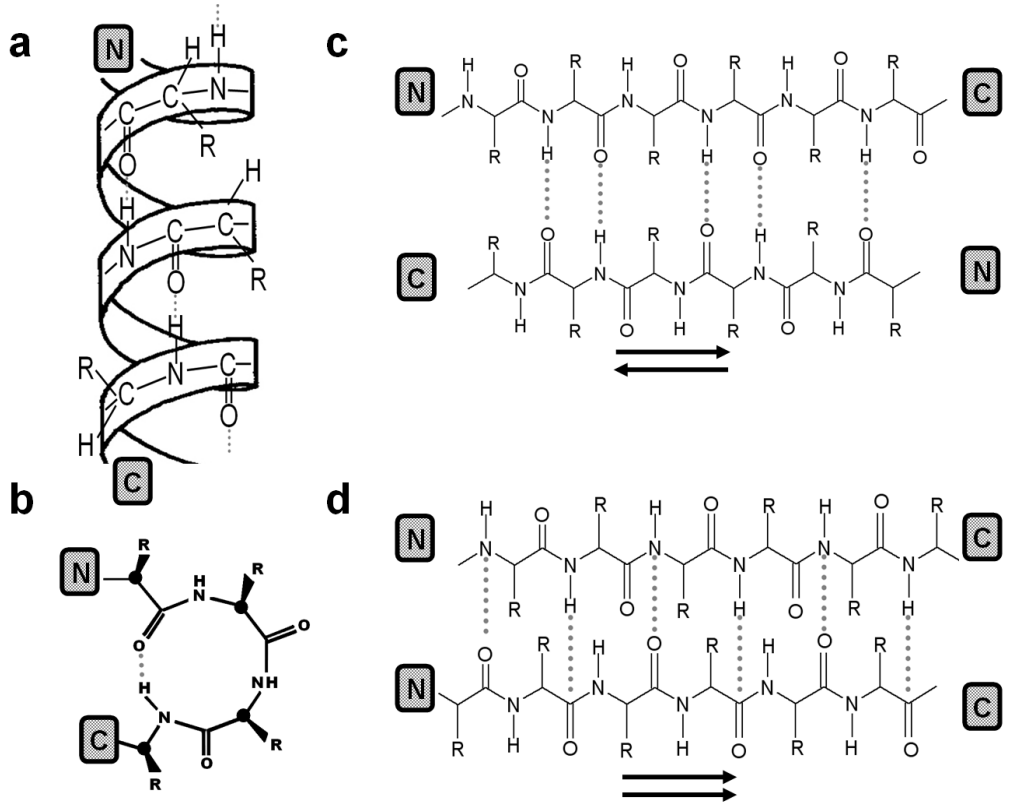


**Figure 1.8** Secondary structure elements of proteins. a: α-helix, b: turn (the black-filled circles represent the $C_\alpha$ atoms in the turn) c: anti-parallel β-sheet, and d: parallel β-sheet. The dotted lines depict the hydrogen bonds. The N in a box corresponds to the N-terminus and the C in a box corresponds to the C- terminus of the proteins. Arrows show the direction of the β-strands in the β-sheets.

A typical α-helix is a right-handed helix with 3.6 amino-acid residues per turn, and a pitch (the distance the helix rises along its axis per turn) of 5.4 Å. In an α-helical structure the backbone hydrogen bonds are arranged such that the C=O bond of the ith amino-acid residue points along the helix axis towards the N-H group of the (i +

4)th amino-acid residue, which results in a strong hydrogen bond. The amino-acid side chains in an α-helix project either outward or downward from the helix. Like the α-helix, the β-sheet uses the full hydrogen-bonding capacity of the polypeptide backbone. However, in β-sheets hydrogen bonding occurs between neighboring polypeptide chains rather than within one chain (compare figure 1.8.a with c and/or d). The β-sheets can be grouped into two different classes: anti-parallel β-sheets, in which neighboring hydrogen-bonded polypeptide chains run in opposite directions (figure 1.8.c) and parallel β-sheets, in which polypeptide chains run in the same direction (figure 1.8.d). Turns are typically stretches of polypeptide chains that can easily change direction (figure 1.8.b). Turns join different α-helices and/or strands of β-sheets in proteins.

### 1.2.2 Misfolding and aggregation of proteins

Protein misfolding and aggregation occurs in biological processes, both in vital and disruptive processes [26]. In contrast to most of the protein aggregates, which are amorphous, some of the protein aggregates generate amyloid fibrils. Amyloid fibrils are about 10 nm in diameter, and are composed typically of 2 to 6 protofilaments [26-28]. Amyloid fibrils of all proteins share a common cross-β structure, wherein the β-strands (figure 1.9.a) are oriented perpendicular to the fibril axis. The β-sheets grow in the direction of the fibril axis by attaching proteins at the ends of the β-sheets (figure 1.9.b). Due to the large size, low solubility, and the noncrystalline nature of fibrils [29], understanding the molecular details of amyloid fibrils has remained a challenge. Amyloid fibrils play a role in neurodegenerative diseases, like Alzheimer's disease and Parkinson's disease [30].

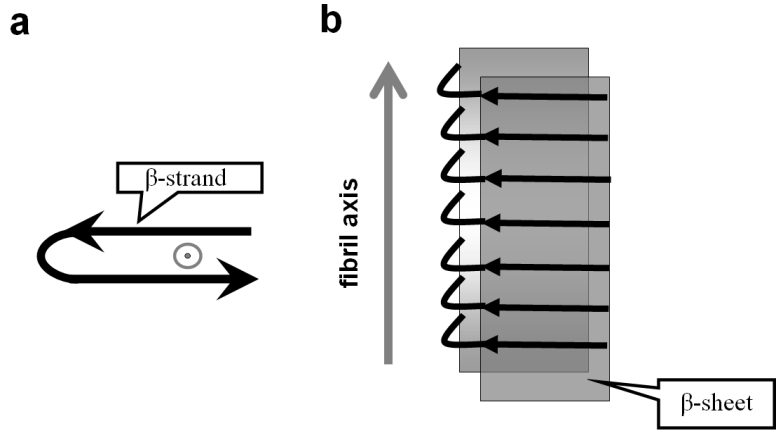


**Figure 1.9** Schematic representation of the structure elements of amyloid fibrils. a: the black arrows show a β-strand and the grey dot shows the direction of the fibril axis, which is pointing out of the page. b: the grey arrow shows the direction of the fibril axis. The grey sheets are representative of β-sheets which are parallel to the fibril axis.

### 1.2.3 Diseases that involve protein misfolding and aggregation

#### 1.2.3.1 Alzheimer's disease: the amyloid β peptide

Alzheimer's disease is the most common neurodegenerative disease in the aging population. Alzheimer's disease is associated with confusion, irritability, aggression, mood swings, trouble with language, progressive cognitive decline, and profound neuronal loss [31-35]. It is characterized by accumulation of intraneuronal neurofibrillary tangles and extracellular senile plaques in the brain tissue and ultimately neuronal and synaptic degeneration [31,33,36,37]. The senile plaques are formed from deposition of the amyloid β (Aβ) peptide in an aggregated fibrillar form.

The Aβ peptide is the product of sequential proteolytic cleavage of the amyloid precursor protein (APP), a transmembrane protein located in the neuronal membrane [38,38,39]. The cleavage of APP is done by α-, β-, and γ-secretases via two distinct pathways: amyloidogenic and non-amyloidogenic [30] (figure 1.10). In the non-amyloidogenic pathway, APP is cleaved by α-secretases and subsequently cleaved by γ-secretases, whereas in the amyloidogenic pathway β-secretase cuts first, followed by γ-secretase cleavage resulting in the amyloid peptides with sequence length ranging from 38 to 43 amino-acid residues. There is evidence for other pathways, involving cleavage of the N-terminus of the Aβ by both α- and β-secretases, which result in the production of several soluble, shorter Aβ fragments in the cerebrospinal fluid [34,38,40,41]. Some of these fragments are up-regulated in Alzheimeer's disease. The aggregation potential of two of these shorter peptides and their influence on the full-length Aβ peptide is investigated in chapter 4.

Soluble Aβ oligomers, rather than fully formed Aβ fibrils and plaques are currently considered as the more likely culprits in cellular toxicity and play an essential role in the pathogenesis of Alzheimer's disease [29,42,43]. The potent pathologic effects of Aβ oligomers provide a compelling reason for elucidating the mechanism(s) leading to the transformation of monomeric Aβ into toxic oligomers and ultimately larger aggregates [44-46]. The hydrophobic part of Aβ suggests a possible membrane activity of the peptide. In chapters 2 and 3 we study and monitor the aggregation process of Aβ on the time scale of EPR in the presence of a membrane mimetic agent.

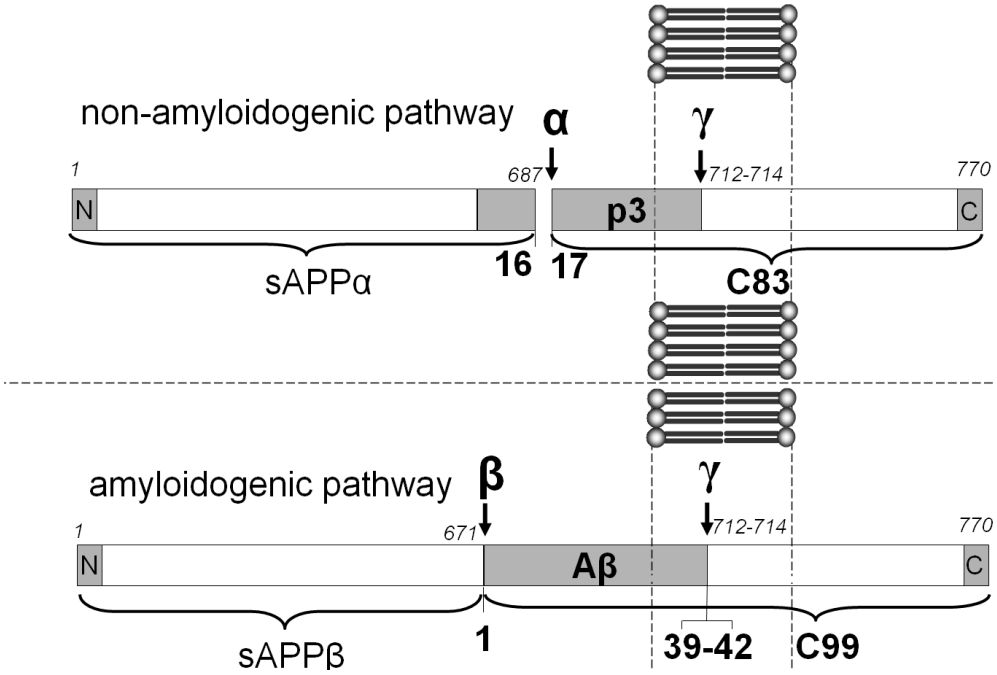


**Figure 1.10** Schematic overview of processing of the amyloid precursor protein (APP). The top panel shows the non-amyloidogenic α-secretase pathway, in which soluble APPα-cleaved (sAPPα) and C83 are generated. Subsequent hydrolysis by the γ-secretase produces a p3 peptide that does not form amyloid deposits. The bottom panel represents the amyloidogenic pathway, in which cleavage of APP by the β-secretase followed by γ-secretase, liberates sAPPβ and C99 and Aβ peptides (Aβ39 to Aβ42) that are found in plaque deposits. *Italics*: sequence numbers of APP protein.

### 1.2.3.2 Parkinson's disease: the α-synuclein protein

Parkinson's disease is the second-most frequent neurodegenerative disorder, which affects more than 1 % of the population above 60 years of age [47]. The most obvious symptoms in Parkinson's disease include tremor, stiffness, slowness of movement, difficulty with walking, and a specific gait. Parkinson's disease is characterized by the accumulation of a neuronal protein, α-synuclein (αS), in Lewy bodies, which are the pathological hallmark of Parkinson's disease. Misfolding and aggregation of the αS protein is accompanied by the loss of dopaminergic neurons in the substantia nigra, a region in the midbrain, and insufficient formation of dopamine, which is important for movement [30,48-50]. The name synuclein arises from the evidence that this protein localizes to synaptic vesicles and portions of the neuronal nucleus [30], but it has also been observed in the cytosol [51,52].
The αS protein (40 kDa) consists of 140 amino-acid residues, of which the N-terminus has a propensity to acquire α-helical structure [53,54]. The central region,

enclosed by amino-acid residues 61 to 95, the so-called NAC region, is hydrophobic and is crucial in the aggregation of αS [55,56] (figure 1.11). The C-terminus of αS is negatively charged and mostly remains unstructured (amino-acid residues 100 to 140). When exposed to phospholipids, detergents or vesicles, αS forms an α11/3 helix, which has 3.67 amino-acid residues per turn instead of 3.6 amino-acid residues per turn of an ideal α-helix [57-60]. This amphiphatic helix allows the αS protein to associate with the surface of membranes [57].

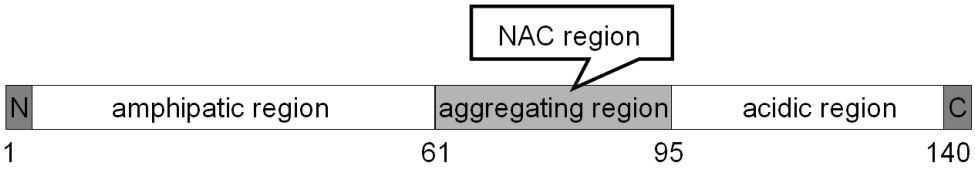


**Figure 1.11** A schematic view of the α-synuclein protein. The highlighted region, amino-acid residues 61 to 95, is reported as the main part involved in the aggregation. The N in a box corresponds to the N-terminus and the C in a box corresponds to the C-terminus of the protein.

Under certain conditions in vitro [58,60] (see chapter 5 of this thesis), αS forms oligomers and ultimately fibrils. The β-sheet core of the fibril starts at amino-acid residues 35-38 and ends around amino-acid residues 89-96 [21,61-64]. The fibrils have a cross-β-sheet structure, which is characterized by x-ray and electron diffraction, in which individual β-strands stack perpendicular to the fibril axis. However, the details of folding and arrangement of aS monomers in the fibrils are still unresolved. In chapter 5 we investigate the fold of αS in the fibril, using distance determination with pulsed EPR.

### 1.2.4 Proteins with disordered regions: the light-harvesting protein CP29

In plants, oxygenic photosynthesis, a process in which solar energy is converted into chemical energy, occurs in the membrane of thylakoids in chloroplasts (figure 1.12). The light-driven charge separation occurs in two chlorophyll-binding protein complexes, photosystem I and photosystem II. The light-harvesting protein CP29 is a member of the photosystem II protein complex machinery. It is located between the major light-harvesting complex LHCII and the core complex [65]. Besides light-harvesting and energy transfer it has a photoprotective function. For light-regulation, CP29 seems to make use of its N-terminus, a stretch of about 100 amino-acid residues. In the recently solved crystal structure of CP29 [65], the N-terminus has no defined electron density. Site-directed spin labeling combined with

EPR enables us to investigate the structure of the disordered N-terminus of CP29. Our study involves two approaches: exploring the mobility of the spin label with continuous wave EPR and distance determination with pulsed EPR. From the present EPR investigation the presence of multiple conformations of the N-terminus is concluded.

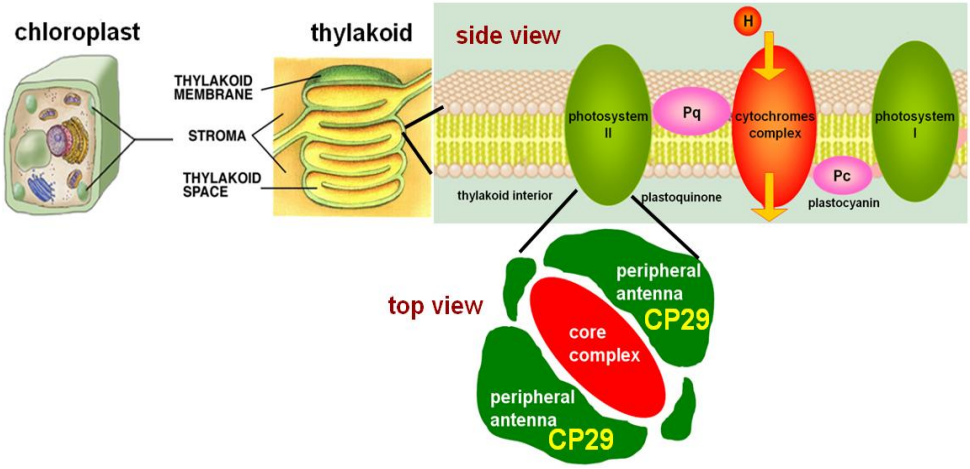


**Figure 1.12** Schematic representation of the location of CP29 in a plant cell, chloroplast.

### 1.3 Thesis outline

This thesis is organized as follows. In chapters 2 and 3 continuous wave (cw) EPR is employed to examine the influence of a membrane-mimetic agent on the aggregation of the Aβ peptide. In chapter 4 the influence of shorter fragments of the Aβ peptide on the aggregation of the full-length Aβ is investigated. In chapter 5 we investigate the fibril fold of the αS protein with pulsed EPR. Chapter 6 describes the structure of the long flexible N-terminus of the light-harvesting antenna protein CP29. In the final chapter we present the EPR characterization of peptides with one or two rigidly-attached spin labels as models for studying spin-spin interaction in distance measurements.

Reference List


[1] A. L. Lehninger, D. L. Nelson, Cox M.M., *Lehninger principles of biochemistry*, 4th ed. W.H. Freeman, New York, **2005**.
[2] L.J.Berliner, J.Grunwald, H.O.Hankovszky, K.Hideg, *Analytical Biochemistry* **1982,** *119* 450-455.
[3] W.L.Hubbell, C.Altenbach, *Current Opinion in Structural Biology* **1994,** *4* 566-573.
[4] W.L.Hubbell, H.S.Mchaourab, C.Altenbach, M.A.Lietzow, *Structure* **1996,** *4* 779-783.
[5] W.L.Hubbell, D.S.Cafiso, C.Altenbach, *Nat.Struct.Biol.* **2000,** *7* 735-739.
[6] H.S.Mchaourab, M.A.Lietzow, K.Hideg, W.L.Hubbell, *Biochemistry* **1996,** *35* 7692-7704.
[7] H.J.Steinhoff, *Frontiers in Bioscience* **2002,** *7* C97-C110.
[8] P.P.Borbat, E.R.Georgieva, J.H.Freed, *J.Phys.Chem.Lett.* **2013,** *4* 170-175.
[9] G.Jeschke, *Annu.Rev.Phys.Chem.* **2012,** *63* 419-446.
[10] O.Schiemann, T.F.Prisner, *Q.Rev.Biophys.* **2007,** *40* 1-53.
[11] P. G. Fajer, in *Encyclopedia of Analytical Chemistry* Ed.: R.A.Meyers, John Wiley & Sons Ltd, Chichester, 2000, **2000**, p. pp. 5725-5761.
[12] P.G.Fajer, *Journal of Physics-Condensed Matter* **2005,** *17* S1459-S1469.
[13] G.Jeschke, *Chemphyschem* **2002,** *3* 927-932.
[14] Atherton N.M., *Principles of Electron Spin Resonance*, Hellis Horwood Limited: Chichester, **1993**.
[15] John A.Weil, James R.Bolton, *Electron Paramagnetic Resonance, Elementary Theory and Practical Applications*, 2nd ed. Wiley-Interscience, A John Wiley & Sons, Inc., **2007**.
[16] R.Owenius, M.Engstrom, M.Lindgren, M.Huber, *Journal of Physical Chemistry A* **2001,** *105* 10967-10977.
[17] Heminga M.A., Berliner L.J., *ESR Spectroscopy in Membrane Biophysics*, Springer, **2007**.
[18] V.Monaco, F.Formaggio, M.Crisma, C.Toniolo, P.Hanson, G.Millhauser, C.George, J.R.Deschamps, J.L.Flippen-Anderson, *Bioorg.Med.Chem.* **1999,** *7* 119-131.
[19] V.Monaco, F.Formaggio, M.Crisma, C.Toniolo, P.Hanson, G.L.Millhauser, *Biopolymers* **1999,** *50* 239-253.
[20] S.Stoll, A.Schweiger, *Journal of Magnetic Resonance* **2006,** *178* 42-55.
[21] A.Der-Sarkissian, C.C.Jao, J.Chen, R.Langen, *J.Biol.Chem.* **2003,** *278* 37530-37535.
[22] S.Bohme, H.J.Steinhoff, J.P.Klare, *Spectroscopy-An International Journal* **2010,** *24* 283-288.
[23] G.Jeschke, A.Bender, H.Paulsen, H.Zimmermann, A.Godt, *J.Magn Reson.* **2004,** *169* 1-12.
[24] G.Jeschke, G.Panek, A.Godt, A.Bender, H.Paulsen, *Applied Magnetic Resonance* **2004,** *26* 223-244.
[25] G.Jeschke, V.Chechik, P.Ionita, A.Godt, H.Zimmermann, J.Banham, C.R.Timmel, D.Hilger, H.Jung, *Applied Magnetic Resonance* **2006,** *30* 473-498.
[26] S.Kumar, S.K.Mohanty, J.B.Udgaonkar, *J.Mol.Biol.* **2007,** *367* 1186-1204.
[27] J.Greenwald, R.Riek, *Structure* **2010,** *18* 1244-1260.
[28] L.C.Serpell, C.C.Blake, P.E.Fraser, *Biochemistry* **2000,** *39* 13269-13275.
[29] E.Herczenik, M.F.Gebbink, *FASEB J.* **2008,** *22* 2115-2133.
[30] P.K.Auluck, G.Caraveo, S.Lindquist, *Annu.Rev.Cell Dev.Biol.* **2010,** *26* 211-233.
[31] R.J.Caselli, T.G.Beach, R.Yaari, E.M.Reiman, *J.Clin.Psychiatry* **2006,** *67* 1784-1800.
[32] K.Chopra, S.Misra, A.Kuhad, *Expert.Opin.Ther.Targets.* **2011,** *15* 535-555.
[33] R.Jakob-Roetne, H.Jacobsen, *Angew.Chem.Int.Ed Engl.* **2009,** *48* 3030-3059.
[34] E.Portelius, N.Mattsson, U.Andreasson, K.Blennow, H.Zetterberg, *Curr.Pharm.Des* **2011,** *17* 2594-2602.
[35] D.J.Selkoe, *Ann.Intern.Med.* **2004,** *140* 627-638.
[36] J.L.Cummings, *N.Engl.J.Med.* **2004,** *351* 56-67.
[37] D.J.Selkoe, *Physiol Rev.* **2001,** *81* 741-766.
[38] E.Portelius, G.Brinkmalm, A.Tran, U.Andreasson, H.Zetterberg, A.Westman-Brinkmalm, K.Blennow, A.Ohrfelt, *Exp.Neurol.* **2010,** *223* 351-358.
[39] M.Gralle, S.T.Ferreira, *Prog.Neurobiol.* **2007,** *82* 11-32.
[40] A.Awasthi, Y.Matsunaga, T.Yamada, *Exp.Neurol.* **2005,** *196* 282-289.

[41] E.Portelius, H.Zetterberg, U.Andreasson, G.Brinkmalm, N.Andreasen, A.Wallin, A.Westman-Brinkmalm, K.Blennow, *Neurosci.Lett.* **2006,** *409* 215-219.
[42] J.Hardy, D.J.Selkoe, *Science* **2002,** *297* 353-356.
[43] H.A.Lashuel, D.Hartley, B.M.Petre, T.Walz, P.T.Lansbury, Jr., *Nature* **2002,** *418* 291.
[44] N.Yamamoto, K.Hasegawa, K.Matsuzaki, H.Naiki, K.Yanagisawa, *J.Neurochem.* **2004,** *90* 62-69.
[45] V.Rangachari, D.K.Reed, B.D.Moore, T.L.Rosenberry, *Biochemistry* **2006,** *45* 8639-8648.
[46] V.Rangachari, B.D.Moore, D.K.Reed, L.K.Sonoda, A.W.Bridges, E.Conboy, D.Hartigan, T.L.Rosenberry, *Biochemistry* **2007,** *46* 12451-12462.
[47] S.I.Shaikh, H.Verma, *Indian J.Anaesth.* **2011,** *55* 228-234.
[48] A.Samii, J.G.Nutt, B.R.Ransom, *Lancet* **2004,** *363* 1783-1793.
[49] L.L.Venda, S.J.Cragg, V.L.Buchman, R.Wade-Martins, *Trends Neurosci.* **2010,** *33* 559-568.
[50] C.W.Hung, Y.C.Chen, W.L.Hsieh, S.H.Chiou, C.L.Kao, *Ageing Res.Rev.* **2010,** *9 Suppl 1* S36-S46.
[51] P.J.Kahle, M.Neumann, L.Ozmen, V.Muller, H.Jacobsen, A.Schindzielorz, M.Okochi, U.Leimer, P.H.van Der, A.Probst, E.Kremmer, H.A.Kretzschmar, C.Haass, *J.Neurosci.* **2000,** *20* 6365-6373.
[52] S.Yu, X.Li, G.Liu, J.Han, C.Zhang, Y.Li, S.Xu, C.Liu, Y.Gao, H.Yang, K.Ueda, P.Chan, *Neuroscience* **2007,** *145* 539-555.
[53] W.S.Davidson, A.Jonas, D.F.Clayton, J.M.George, *J.Biol.Chem.* **1998,** *273* 9443-9449.
[54] D.Eliezer, E.Kutluay, R.Bussell, Jr., G.Browne, *J.Mol.Biol.* **2001,** *307* 1061-1073.
[55] B.I.Giasson, I.V.J.Murray, J.Q.Trojanowski, V.M.Y.Lee, *Journal of Biological Chemistry* **2001,** *276* 2380-2386.
[56] H.Miake, H.Mizusawa, T.Iwatsubo, M.Hasegawa, *J.Biol.Chem.* **2002,** *277* 19213-19219.
[57] M.Mihajlovic, T.Lazaridis, *Proteins* **2008,** *70* 761-778.
[58] M.Drescher, F.Godschalk, G.Veldhuis, B.D.van Rooijen, V.Subramaniam, M.Huber, *Chembiochem* **2008,** *9* 2411-2416.
[59] M.Drescher, B.D.van Rooijen, G.Veldhuis, V.Subramaniam, M.Huber, *J.Am.Chem.Soc.* **2010,** *132* 4080-4082.
[60] M.Drescher, M.Huber, V.Subramaniam, *Chembiochem* **2012**.
[61] M.Chen, M.Margittai, J.Chen, R.Langen, *J.Biol.Chem.* **2007,** *282* 24970-24979.
[62] G.Comellas, L.R.Lemkau, A.J.Nieuwkoop, K.D.Kloepper, D.T.Ladror, R.Ebisu, W.S.Woods, A.S.Lipton, J.M.George, C.M.Rienstra, *J.Mol.Biol.* **2011,** *411* 881-895.
[63] H.Heise, W.Hoyer, S.Becker, O.C.Andronesi, D.Riedel, M.Baldus, *Proc.Natl.Acad.Sci.U.S.A* **2005,** *102* 15871-15876.
[64] M.Vilar, H.T.Chou, T.Luhrs, S.K.Maji, D.Riek-Loher, R.Verel, G.Manning, H.Stahlberg, R.Riek, *Proc.Natl.Acad.Sci.U.S.A* **2008,** *105* 8637-8642.
[65] X.Pan, M.Li, T.Wan, L.Wang, C.Jia, Z.Hou, X.Zhao, J.Zhang, W.Chang, *Nat.Struct.Mol.Biol.* **2011,** *18* 309-315.